Research Article | Open Access

Microstructures

Kikuchi *et al. Microstructures* **2026**, *6*, 68 **DOI:**10.20517/microstructures.2025.116

# Deformation analysis of harmonic structured high-entropy CrMnFeCoNi alloy during *in-situ* tensile tests using micro-digital image correlation

**Shoichi Kikuchi[1], Shinnosuke Baba[2], Masaki Katsumata[2], Mie Ota Kawabata[3], Hiroshi Fujiwara[3], Kei Ameyama[3]**

**Keywords:**
High-entropy alloy, heterogeneous structure, powder metallurgy, grain refinement, micro-digital image correlation, strain partitioning

**Citation:** Kikuchi, S.; Baba, S.; Katsumata, M.; Kawabata, M. O.; Fujiwara, H.; Ameyama, K. Deformation analysis of harmonic structured high-entropy CrMnFeCoNi alloy during *in-situ* tensile tests using micro-digital image correlation. *Microstructures* **2026**, *6*, 68. https://dx.doi.org/10.20517/microstructures.2025.116

**Received:** 31 Jul 2025 **First Decision:** 29 Aug 2025 **Revised:** 10 Oct 2025 **Accepted:** 15 Oct 2025 **Published:** 18 May 2026

**Academic Editors:** Xiaozhou Liao, Xiaolei Wu **Copy Editor:** Shu-Yuan Duan **Production Editor:** Shu-Yuan Duan

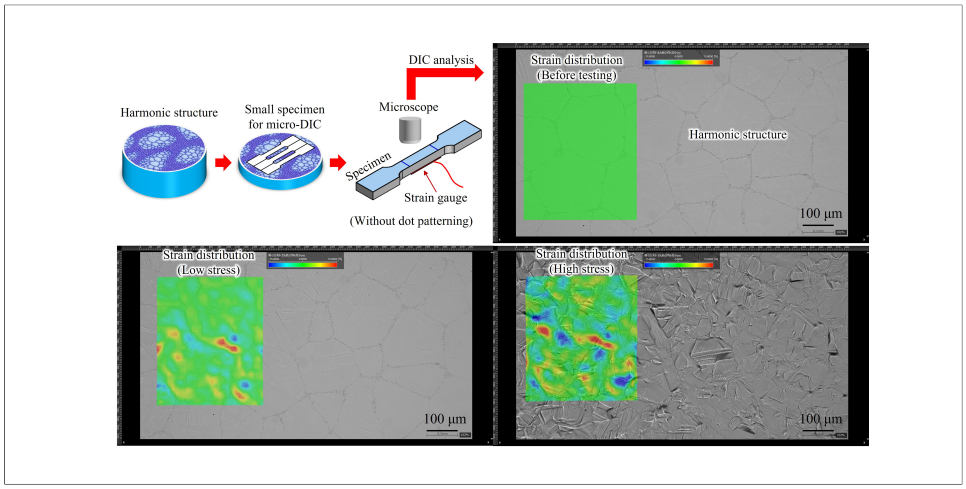


## Abstract

There is a trade-off relationship between strength and ductility in the case of homogeneous crystalline metals. This work assessed the deformation characteristics of a high-entropy CrMnFeCoNi alloy having a harmonic structure, defined as a coarse-grained structure surrounded by a network of fine grains to solve this problem. These evaluations were performed by *in situ* tensile tests using micro-digital image correlation (micro-DIC). Mechanically milled CrMnFeCoNi powder was consolidated at 1,273 K by spark plasma sintering to fabricate the harmonic structured alloy. The microstructure of this material was characterized by optical microscopy and electron backscatter diffraction while the micro-hardness distribution was obtained from Vickers hardness tests. Micro-DIC analyses were able to determine strain distributions without dot patterning based on microstructural heterogeneity. Pronounced strain partitioning was observed and high strain peaks were generated near the boundaries between fine- and coarse-grained structures. Fracture surface observations using scanning electron microscopy confirmed that cracks were initiated within the fine-grained structures due to stress partitioning, as verified by finite



[1]Department of Mechanical Engineering, Shizuoka University, Hamamatsu 4328561, Japan.
[2]Graduate School of Science and Technology, Shizuoka University, Hamamatsu 4328561, Japan.
[3]Department of Mechanical Engineering, Ritsumeikan University, Kusatsu 5258577, Japan.

**Correspondence to:** Dr. Shoichi Kikuchi, Department of Mechanical Engineering, Shizuoka University, Hamamatsu 4328561, Japan. E-mail: kikuchi.shoichi@shizuoka.ac.jp

element analysis. Thus, in contrast to homogeneous course-grained alloys, a harmonic structured CrMnFeCoNi specimen was able to exhibit both high strength and high ductility.

## INTRODUCTION

High-entropy alloys (HEAs) are metals typically comprising five or more main elements in equiatomic proportions. Various such materials have recently been developed and improved based on compositional optimization, as a means of enhancing mechanical properties[1,2]. Cantor *et al.* devised a series of typical HEAs having the formula CrMnFeCoNi[3] that exhibited face-centered cubic (fcc) structures and superior mechanical properties even at cryogenic temperatures[4,5]. However, as with other metallic materials, an HEA having a coarse-grained structure will possess relatively low strength[4]. As such, grain refinement through severe plastic deformation or heat treatment is often required to produce a high strength HEA[6-8] on the basis of the Hall-Petch effect.

Unfortunately, there is a trade-off relationship between strength and ductility in the case of homogeneous crystalline HEAs[7], as is also true for conventional metals[9-12]. For this reason, heterogeneous microstructures induced by heat treatment or powder metallurgy have been studied as approaches to increasing both strength and ductility[11-18]. On this basis, the novel concept of a heterostructure, otherwise known as a harmonic structure (HS), has been proposed by Ameyama *et al.*[19]. An HS is a coarse-grained morphology surrounded by a network of fine grains and can be generated by sintering metallic powders following severe plastic deformation via powder metallurgy. The present authors previously examined the mechanical properties of various metallic materials having such structures[19]. An HS has been found to improve both the strength and ductility of fcc austenitic stainless steels by inducing a unique deformation mechanism that prevents necking during tensile tests[19]. Orlov *et al.* also observed clear strain partitioning between fine- and coarse-grained structures during the plastic deformation of materials having HSs[20].

Previous studies reported the production of HEAs with fcc HSs and demonstrated that the coarse grain regions showed higher plastic strain values compared with the fine grain areas, resulting in strain partitioning between these regions in response to static tension[21]. In addition, Shi *et al.*[22] found that the crack closure effect is not significantly related to the crack tip plasticity and fatigue crack propagation is impeded by the relatively coarse-grained structure; therefore, fatigue cracks deflect at the boundaries between fine and coarse grains in HEAs having HSs under cyclic loading with plastic deformation. In contrast, fatigue cracks tend to begin within coarse-grained structures in standard HS metals in response to cyclic loading with elastic deformation (high-cycle fatigue region)[19]. This prior work suggests that the mechanical properties of materials having HSs can be greatly modified as a result of plastic deformation, due to the presence of both fine- and coarse-grained structures in these metals. It would thus be beneficial to assess the unique plastic deformation characteristics associated with HSs based on differentiating the deformation properties of fine- and coarse-grained regions in HEAs.

The present study examined the deformation of an CrMnFeCoNi alloy having an HS by performing *in situ* tensile tests in conjunction with micro-digital image correlation (micro-DIC). The mechanism associated with the fracturing of this alloy under monotonic tension was also elucidated using fractography and stress analysis.

## MATERIALS AND METHODS

### Materials

The CrMnFeCoNi HEA was initially processed into a powder having a mean particle diameter of 202 μm, which was obtained by the image analysis using the WinROOF2023 software, using a plasma-based rotating electrode process[23]. Figure 1A and B show the frequency distribution and cumulative frequency distribution

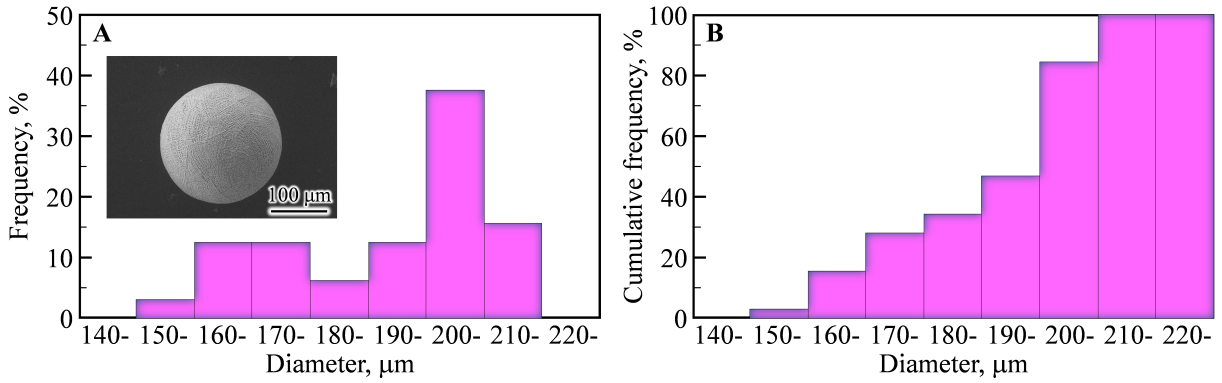


**Figure 1.** (A) Frequency distribution and (B) cumulative frequency distribution of as-received CrMnFeCoNi powders.

of as-received CrMnFeCoNi powders used in this study. Following this, mechanical milling (MM) and spark plasma sintering (SPS) were used to produce an HS in the alloy. The MM of the CrMnFeCoNi powder was first conducted for a duration of 180 ks under argon at room temperature without using the process control agent (PCA). This process used a planetary ball mill with steel ball bearings and a tungsten carbide vessel to refine the grains at the particle surfaces. The rotational rate was 3.3 Hz and the ball-to-powder mass ratio was 2:1. The resulting powder was then consolidated by SPS at 1,273 K for 3.6 ks under vacuum with the application of a pressure of 100 MPa, using graphite dies each with an internal diameter of 25 mm (referred to herein as the Harmonic series). For comparison purposes, CrMnFeCoNi compacts having homogeneous coarse grains were also prepared by sintering portions of the as-received CrMnFeCoNi powder. These specimens are referred to as the Homo series herein. The microstructures of the sintered compacts were observed using optical microscopy and analyzed using electron backscatter diffraction (EBSD).

## Testing and specimens

Figure 2A and B present photographic images of the custom-made tensile testing system allowing *in situ* observations used in the present work. This set-up consisted of an optical microscope equipped with a long working distance lens and a tensile testing apparatus. Figure 2C presents a diagram of the specimen shape used for the tensile tests. In preparation for analysis, each of the sintered materials was cut to a thickness of approximately 0.7 mm and then machined to produce a tensile specimen having these dimensions. The specimen surfaces were subsequently polished with emery paper and a $SiO_2$ suspension to obtain a mirror finish. The macroscopic strain was monitored during tensile tests using a dynamic strain recorder. This was accomplished by attaching a strain gauge to the back surface of the specimen, as shown in Figure 2B. Lines were inscribed 6.5 mm apart from one another using a height gauge on the mirror-finished surface of the specimen to allow the elongation to be determined based on measuring the distance between the lines after testing. It was confirmed that final fracture of specimens did not occur near the lines; therefore, local plastic deformation/stress concentration near the lines does not affect the subsequent DIC results in this study.

Using this apparatus, the tensile tests were conducted at a loading rate of 0.2 mm/min under ambient conditions on the stage of the optical microscope, as shown in Figure 2A. During each trial, this microscope was used to capture images of the specimen surface at a resolution of 3,840 × 2,160 pixels and a rate of 30 fps. The resulting images were analyzed using the DIPP-Strain software package (DITECT Corporation) with each pixel equal to a size of 0.28 μm, employing a subset size of 131 × 131 pixels, subset spacing of 45 × 45 pixels and a gauge length of 40 pixels. It cannot follow the deformation of the microstructure during tensile tests when the subset size is too small, whereas the strain of the fine- and coarse-grained regions cannot be measured separately when the subset size is too large. Therefore, these parameters for a DIC assessment were determined through trial and error by confirming that the strain values obtained using the strain gauge

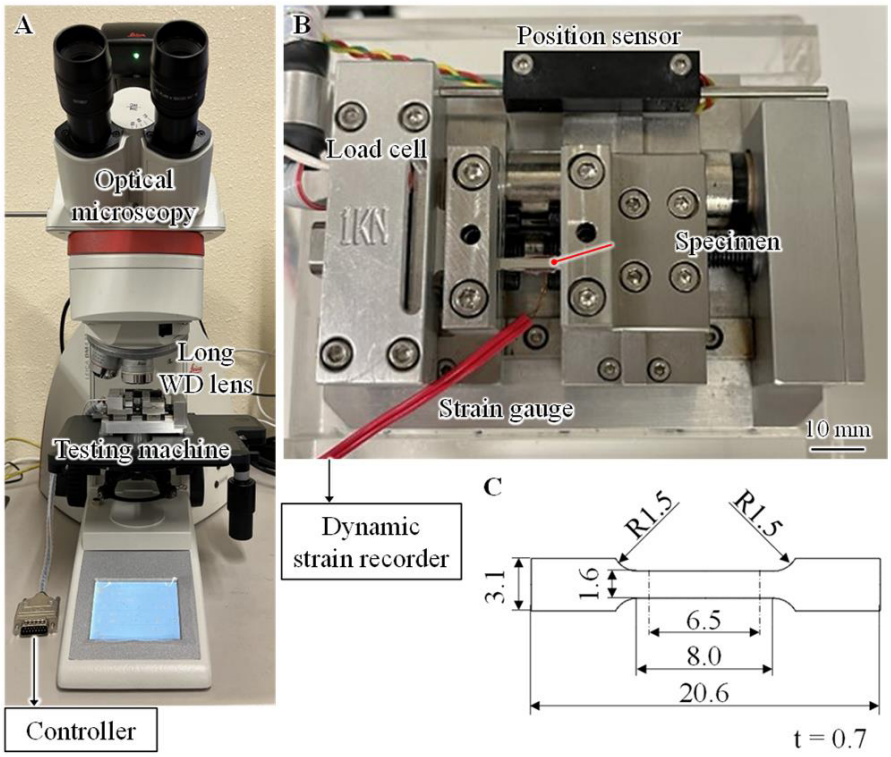


**Figure 2.** (A and B) *In-situ* tensile testing system; (C)specimen configuration (units: mm). WD: Working distance.

match the average strain values in the DIC analyzed area. Although random patterns are typically applied to the specimen surface prior to a DIC assessment, analysis of the present HS specimens using micro-DIC was performed without dot patterning. This was possible because the heterostructure and shading inherent to the HS could be used as patterns, as discussed further on. Using this test system, the strain distribution in an HEA having an HS could be assessed under tension. After testing, fracture and intact surfaces were observed using scanning electron microscopy (SEM) and optical microscopy to elucidate the fracture mechanism.

The Homo and Harmonic series were both subjected to Vickers hardness testing at a relatively low load of 0.049 N, with a load hold time of 10 s. The aim was to examine differences in hardness between the fine- and coarse-grained structures in these materials. Following tensile testing, some specimens were also analyzed using EBSD to look for correlations between the hardness distribution and microstructure of each.

## Finite element analysis

Finite element analysis (FEA) was conducted to evaluate the stress partitioning behavior of the Harmonic series. Figure 3 shows the FEA model for the Harmonic series. In this study, ANSYS-2020R2 software was used and the shape of the element was selected as tetrahedron. The harmonic structure obtained through microstructural characterization; including DIC analyzed area and EBSD analyzed area as discussed later, were constructed into FEA models. Force was applied incrementally to one side of the FEA model.

The local 0.2% proof stresses of fine- and coarse-grained regions were estimated from the Hall-Petch relationship. The local 0.2% proof stresses of both regions were incorporated into the FEA model as the two-line approximation plasticity model. However, grain boundaries were not considered in this model because the aim is to mainly examine the effect of the network structure in the Harmonic series on the stress partitioning behavior of HEAs in this study.

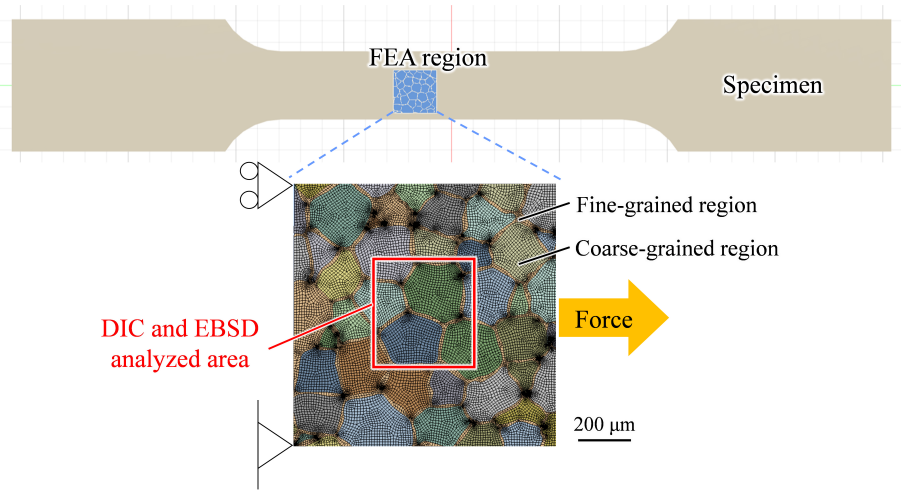


**Figure 3.** FEA model for Harmonic compact. FEA: Finite element analysis; DIC: digital image correlation; EBSD: electron backscatter diffraction.

## RESULTS AND DISCUSSION

### Microstructural characterizations

Figure 4 shows image quality (IQ) maps obtained from EBSD analyses together with optical micrographs acquired from the HS specimen in the same field of view at low and high magnifications. A coarse-grained structure surrounded by a network of fine grains, matching the definition of an HS, can be clearly seen in Figure 4A and C. The EBSD results also establish that the coarse-grained structure comprised crystalline grains with sizes on the order of tens of microns [Figure 4B], whereas the fine-grained structure consisted of a network of crystal grains with sizes on the order of several microns [Figure 4D]. Table 1 summarizes the average grain size of the sintered compacts with respect to the entire microstructure, fine-grained structure, coarse-grained structure, and the areal fraction of the fine-grained microstructure. In the present study, fine grains are defined as grains smaller than 10 μm and coarse grains are defined as grains 10 μm or larger. The average grain size of the Harmonic series was smaller than that of the Homo series. This is because grain refinement occurs at the powder particle surfaces due to an increase in the strain induced by MM. Furthermore, the average coarse-grain size of the Harmonic series was also smaller than that of the Homo series, which implies that the microstructure at the center of powder particles also becomes slightly fine during MM. The IQ maps and the optical micrographs show consistent patterns at the same magnifications. As described further on, these features derived from the HS allowed micro-DIC analysis without imparting dot patterns to the tensile specimens.

### Mechanical properties

The Vickers hardness values of the sintered compacts were determined to investigate the effect of HS on the hardness distribution of the HEA. Figure 5A presents hardness profiles for the Homo and Harmonic compacts. The hardness values for the latter specimen, which was manufactured by consolidating a powder after MM, were found to vary as a function of position. In contrast, the hardness values of the Homo compact, which had a homogeneous coarse grain structure, were essentially constant. It is also evident that the hardness of the HS material was significantly increased at the points labeled (i)-(iii) in Figure 5A.

The cause of the hardness variations associated with the HS sample was investigated by performing a further EBSD analysis of the Harmonic compact after hardness testing. Figure 5B provides the IQ map of the specimen corresponding to the hardness testing area, which clearly shows the indentation marks and the HS. It is apparent that the hardness values of the fine-grained structures at locations (i)-(iii) were higher than

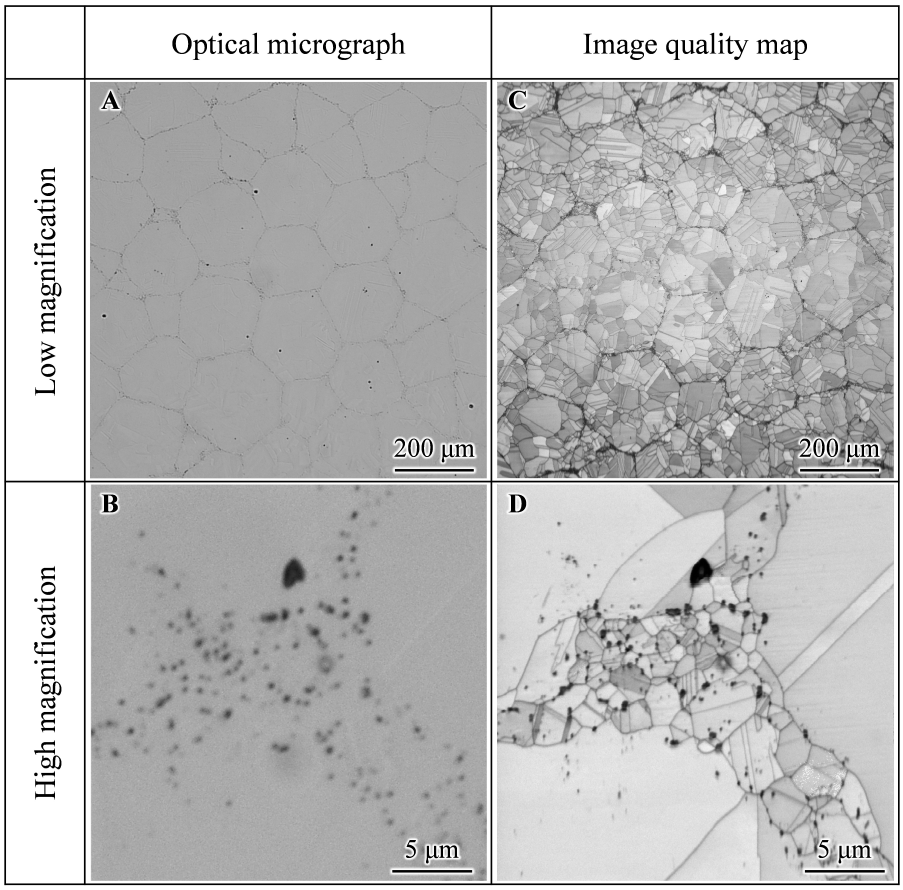


**Figure 4.** (A and B) Optical micrographs and (C and D) IQ maps of Harmonic compact acquired in same field of view at different magnifications. IQ: Image quality.

**Table 1. Average grain size and areal fraction of the fine-grained structure in sintered compacts**

| Specimen series | Homo | Harmonic |
|---|---|---|
| Average grain size in entire microstructure, µm | 17.8 | 7.1 |
| Average grain size in fine-grained structure, µm | 5.9 | 3.5 |
| Average grain size in coarse-grained structure, µm | 25.5 | 20.7 |
| Areal fraction of fine-grained structure, % | 2.8 | 11.0 |

those of the coarse-grained structures. This result suggests that these unique hardness variations stemmed from hard fine-grained structure and soft coarse-grained structure in the HS.

Figure 6 summarizes the results of tensile testing of the HEA compacts. Figure 6A presents stress-strain curves while Figure 6B shows the relationship between nominal stress and cross-head displacement. The former data confirm that the 0.2% proof stress of the Harmonic compact (267.1 MPa) was higher than that of the Homo compact (246.1 MPa). Figure 6B reveals that the ultimate tensile strength of the former (596.9 MPa) was also greater than that of the latter (569.1 MPa). From these results, it is evident that the HEA having an HS exhibited higher strength compared with the homogeneous coarse-grained counterpart. In addition, the crosshead displacement in the tensile stage of the Harmonic compact was higher than that of the Homo compact. Measuring the distance between the inscribed lines on the specimens before and after testing demonstrated that the elongation of the HEA sample was increased from 43.8% to 50.0% after imparting an HS to the metal. Hence, the HS appears to have increased the strength of the HEA without

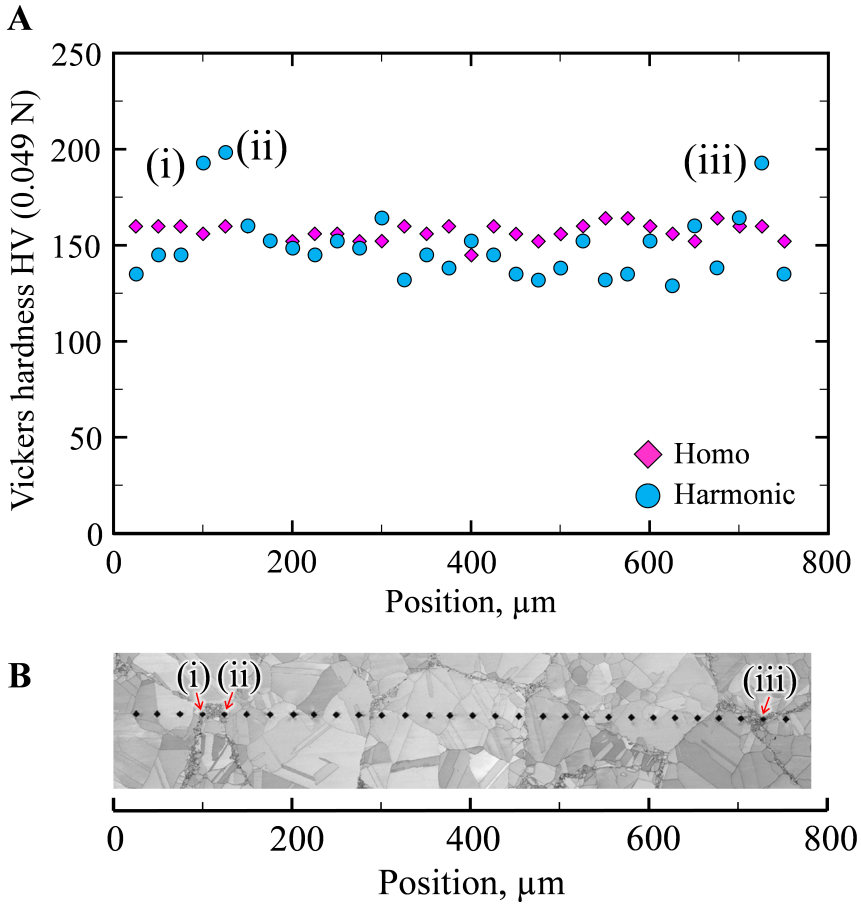


**Figure 5.** (A) Vickers hardness distributions for Homo and Harmonic specimens and (B) IQ map for Harmonic compact. IQ: Image quality.

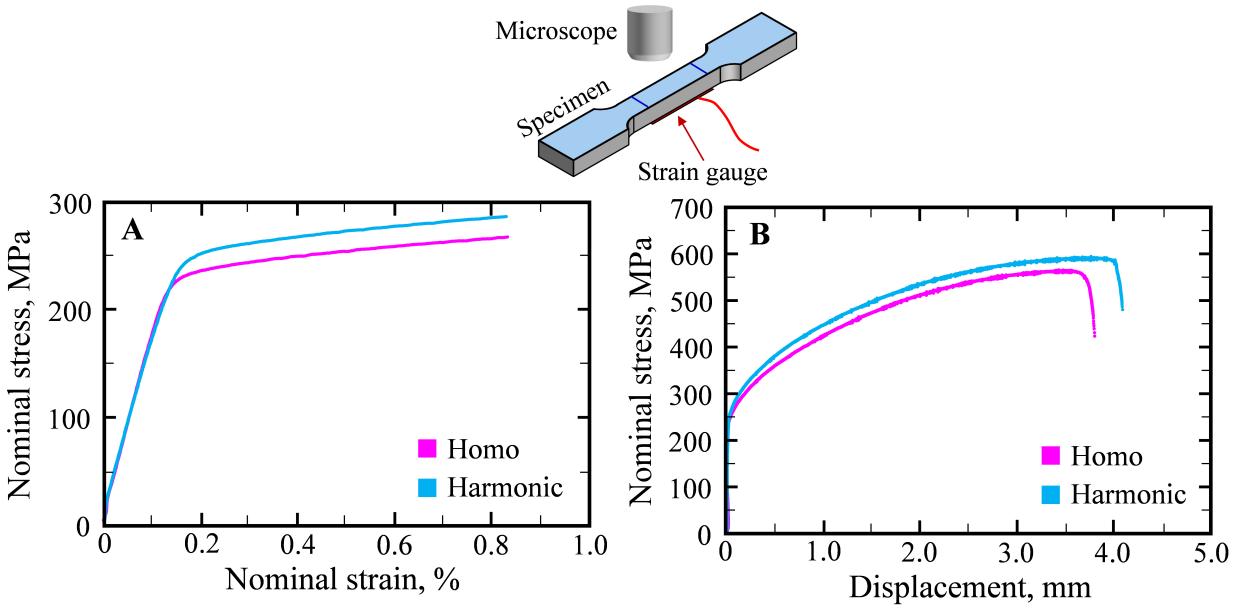


**Figure 6.** (A) Stress-strain curves and (B) stress-displacement curves for Homo and Harmonic specimens together with diagram of test specimen.

lowering the ductility of the material. Similar trends have been observed in CrMnFeCoNi alloys having HSs[21], although the areal fraction and size of the fine-grained structure were different in the HS. Then, it is inferred that the improvement of strength by HSs was not significant because the areal fraction of fine grains was not large as shown in Table 1.

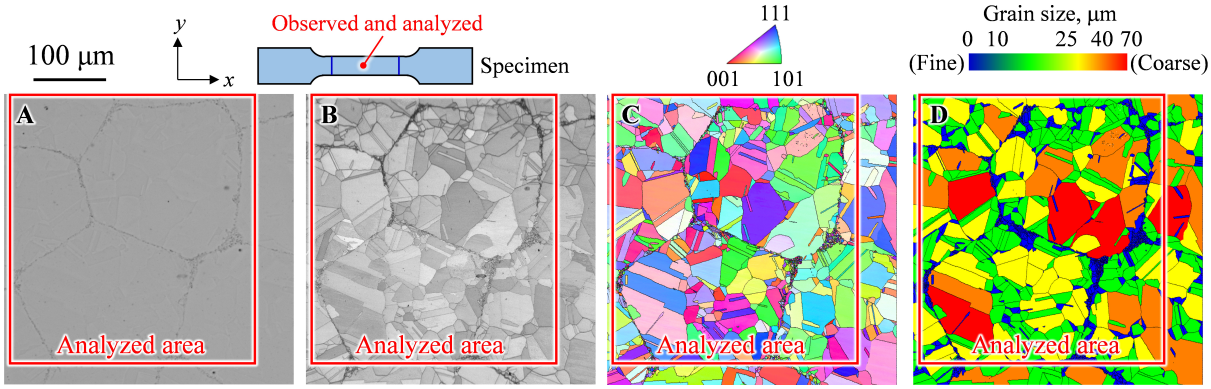


**Figure 7.** (A) Optical micrograph; (B) IQ map; (C) IPF map and (D) grain size map for Harmonic compact within same field of view. IQ: Image quality; IPF: inverse pole figure.

These results indicate that imparting an HS to the HEA increased both the strength and ductility of the alloy. To examine the extra strengthening effect due to an HS, the 0.2% proof stress of the Harmonic series was estimated based on a rule of mixtures. In this estimation, the 0.2% proof stress of the Homo series having coarse-grains (246.1 MPa), the areal fraction of the fine-grains (11.0%), the average hardness of the Homo series having coarse-grains [157.5 Vickers Hardness (HV)] and the average hardness of fine-grains in the Harmonic series (194.9 HV) were used. As results, the estimated 0.2% proof stress of the Harmonic series (252.5 MPa) was lower than that obtained by the tensile test (267.1 MPa). This result suggests that the extra strengthening effect due to the HS design was observed in the HEAs. The cause of high ductility due to HSs is investigated in the next section.

## Analysis of strain partitioning by micro-DIC

As discussed, the HEA having an HS exhibited superior mechanical properties. The reason for the increased elongation of this specimen was examined using micro-DIC analysis. Prior to these assessments, the microstructure of the Harmonic compact was observed and analyzed. Figure 7 presents an optical micrograph, IQ map, inverse pole figure (IPF) map and grain size map of the Harmonic compact, all acquired within the same field of view. In this figure, the red squares indicate the region analyzed by micro-DIC. No random patterns were assigned because the microstructure of the Harmonic compact, whose heterogeneity was used in the micro-DIC analysis, reflects the local strain distribution as discussed below.

Figure 8 provides superimposed optical micrographs and x-direction normal strain, $\varepsilon_{xx}$, and shear strain, $\varepsilon_{xy}$, maps obtained from the micro-DIC analysis of the Harmonic compact in the region corresponding to the red squares in Figure 7. In Figure 8A-A', a non-uniform strain distribution can be seen to have been generated at a macroscopic strain of 0.10%, although Young's modulus was constant independent of changes in the grain size. Interestingly, high strains were observed near the boundaries between fine- and coarse-grained structures, as indicated by the red arrows in Figure 8Aand A'. At a macroscopic strain of 0.59%, the local strain values observed near the boundaries between the fine- and coarse-grained structures were increased [Figure 8B and B']. In addition, slip bands or twin boundaries appeared as a result of plastic deformation, in agreement with the EBSD data shown in Figure 8B-D'. A macroscopic strain of 1.5% increased the local strain values near the boundaries between the fine- and coarse-grained structures while the formation of slip bands or twin boundaries became more pronounced [Figure 8C and C']. Furthermore, high strain values were observed near the grain boundaries inside the coarse-grained structures, as indicated by the blue arrows in Figure 8C and C'. Thus, significant strain partitioning occurred in the Harmonic compact. At macroscopic strains of 3.8%, 7.0% and 10%, the region within which high strain was induced became wider [Figure 8D-F'].

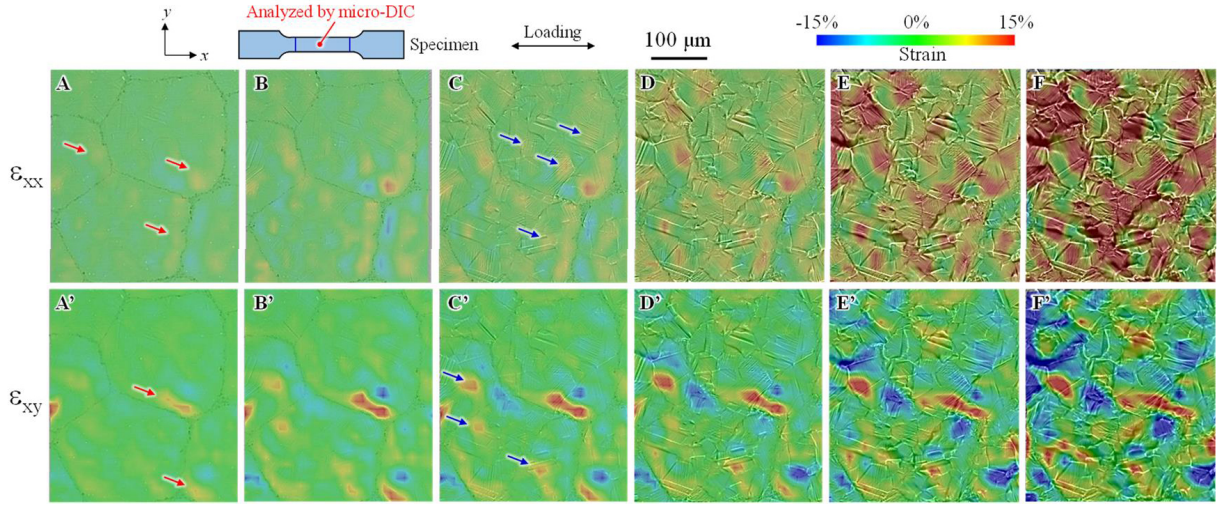


**Figure 8.** Strain ($\varepsilon_{xx}$ and $\varepsilon_{xy}$) maps obtained by micro-DIC for Harmonic compact at macroscopic strains of (A and A') 0.10%; (B and B') 0.59%; (C and C') 1.5%; (D and D') 3.8%; (E and E') 7.0% and (F and F') 10%. $\varepsilon_{xx}$: Normal strain; $\varepsilon_{xy}$: shear strain; DIC: digital image correlation.

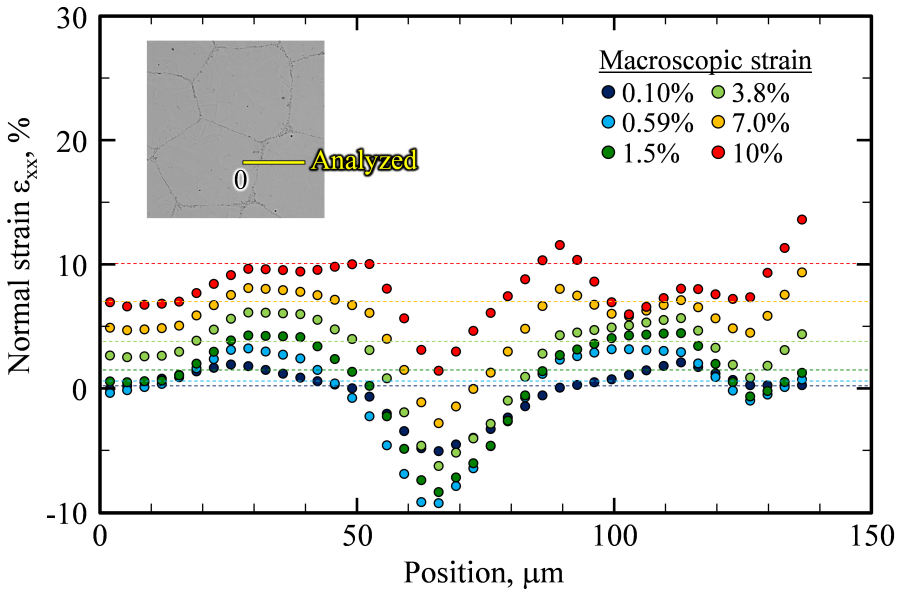


**Figure 9.** Normal strain ($\varepsilon_{xx}$) profiles near the boundaries between fine- and coarse-grained structures obtained by micro-DIC for Harmonic compact. DIC: Digital image correlation.

Figure 9 shows the x-direction normal strain, $\varepsilon_{xx}$, profiles obtained near the boundaries between fine- and coarse-grained structures under various macroscopic strain conditions. As macroscopic strain increased, maximum strain values tended to increase. In addition, strain values varied as a function of position and maximum strain values were higher than the macroscopic strain represented by dotted lines. Particularly, high strains were observed near the boundaries between fine- and coarse-grained structures. The strain gradient due to strain partitioning was quantitatively examined by the micro-DIC analysis.

The concept of geometrically necessary dislocations (GNDs) should be introduced because the strain gradient, which was observed in the strain map obtained by the DIC analysis, needs to be accommodated by GNDs. Zhu *et al.* proposed the concept of hetero-deformation induced (HDI) hardening for HS materials[24].

A GND pileups against the domain boundary in the soft coarse grains in HS materials under an applied shear stress, which produces back stress in the opposite direction of the applied shear stress in the soft domain to make it appear stronger. Then, a stress concentration at the head of the pile-up is applied to the hard fine-grains across the domain boundary, which is in the same direction of the applied stress; named forward stress. The back stress in the soft coarse-grained regions induced the forward stress in the hard fine-grained regions. In practice, mechanical incompatibility can be induced in an HEA having an HS as the soft coarse-grains start to deform plastically during the early stages of strain while the hard fine-grains undergo elastic deformation as a result of the high strength in the fine-grain regions. This occurs even though the Young's modulus will be independent of grain size. The soft coarse-grains cannot deform freely due to the restriction from the network of hard fine-grains, leading to strain gradients near the boundaries between fine- and coarse-grain regions. This phenomenon is based on the variations in ductility and the drive for constant strain throughout the specimen. The hetero-deformation that leads to the generation of back stress and forward stress, which collectively induces the extra strengthening; HDI hardening, as discussed in the previous section. Consequently, both the coarse- and fine-grained regions undergo plastic deformation, although the coarse grains are able to endure higher plastic strains than the fine grains, resulting in strain partitioning between the regions. The results obtained in this study are therefore consistent with previous report[19].

As noted, micro-DIC analysis could be used to assess the present CrMnFeCoNi having an HS, as a means of ascertaining the strain distribution, without dot patterning because of the heterogeneous microstructure. The data indicate that the most important factor determining strain partitioning in the HS was the boundaries between coarse- and fine-grained structures, while the second most important factor was the grain boundaries in the HS.

## Fracture mechanism

Fractography was used to examine the fracture mechanism associated with the present HEA having an HS, as a means of understanding the increased strength of this material. Figure 10A and B show SEM micrographs of the fracture surfaces of the Harmonic compact acquired at low and high magnifications. On this macroscopic scale, this specimen clearly had a rough surface [Figure 10A] and the surface morphology reflects the sizes of the HEA particles following the MM process. The relative density of the HS material as determined by the Archimedes method was 97.5% and no pores were observed on the sintered compact during SEM observations. These findings, together with the SEM images, suggest that the HEA failed near the boundaries between the fine- and coarse-grained structures. It should also be noted that dimples were observed on the fracture surface on a microscopic scale within both the fine- and coarse-grained structures, meaning that this material underwent ductile fracture.

Figure 10C and D provide SEM micrographs of the surface of the Harmonic compact after failure, acquired at low and high magnifications. It is apparent that cracks propagated along the fine-grained structure in the metal. As discussed in the previous section, strain partitioning occurred in the HS material due to variations in ductility. On the same basis, stress partitioning also occurred near the boundaries between fine- and coarse-grains in the HS because the fine- and coarse-grained structures had different strengths. FEA for an HEA having an HS confirmed that higher stress would have been applied to the fine-grained structures because these regions had higher 0.2% proof stress values than the coarse-grained areas as discussed below. The occurrence of stress partitioning in HS materials has been observed in previous studies[19,20]. Thus, cracks are thought to have been initiated within the fine-grained structures due to stress partitioning.

Further information concerning the fracture mechanism was obtained by making similar observations in the center of a specimen. Figure 11A shows an SEM micrograph of the fracture surface of a Harmonic compact, the thickness of which had been reduced by polishing. The fracture surface seen here is equivalent to that in

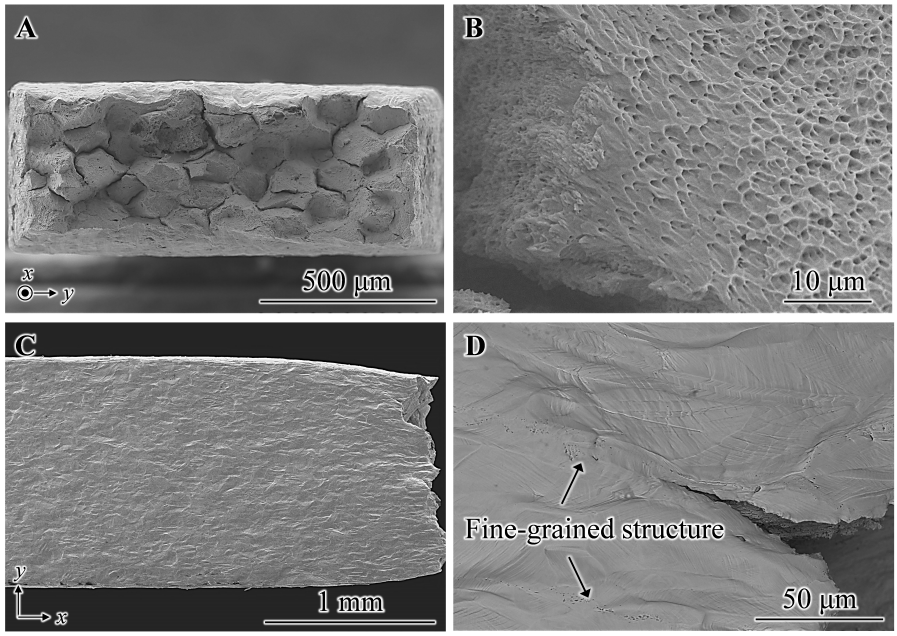


**Figure 10.** (A and B) SEM micrographs of fracture surface and (C and D) the surface after failure of Harmonic compact observed at low and high magnifications. SEM: Scanning electron microscopy.

Figure 10A except for the thickness of the specimen. Figure 11B and C establishes that the fracture surface morphology reflected the diameters of the HEA particles. Figure 11D-F provide optical micrographs of the specimen's surface within the same field of view as the fracture surface. These images confirm that the shape of the fracture surface corresponded to both micrographs and that cracks propagated along the fine-grained structure. It is apparent that cracks also propagated near the triple point of the network structure within the fine-grained region, as indicated by the arrows. Our previous study investigated the fracture and deformation of stainless steel specimens having harmonic microstructures using detailed SEM observations, and found that cracks propagated along interfaces between fine and coarse grains.

To examine the fracture of the fine-grained regions in the Harmonic series, FEA was conducted for the Harmonic series. Figure 12 shows the equivalent stress maps obtained by FEA for Harmonic compact under various stress conditions corresponding to macroscopic strains shown in Figure 8. In this figure, the red squares correspond to the region analyzed by micro-DIC. In Figure 12A and A', a non-uniform stress distribution can be seen to have been generated at a macroscopic strain of 0.10% in elastic region, because Young's modulus was constant independent of changes in the grain size. In contrast, at a macroscopic strain of 0.59%, the high stress values were observed in the network structure of the fine grains which has higher 0.2% proof stress [Figure 12B and B']. Thus, significant stress partitioning occurred in the Harmonic compact. As a macroscopic strain increased, stress partitioning became more pronounced [Figure 12C-F']. If the areal fraction of the fine-grained structure, stress partitioning behavior would be changed. We can control the harmonic structure fraction by changing the milling time[22]; therefore, comparisons with different HS fractions will be addressed in future.

Consequently, cracks were initiated at the fine-grained structure in the Harmonic series due to stress partitioning, although fine grains exhibited high strength.

An illustration of the proposed fracture mechanism for a harmonic structured HEA is shown in Figure 13. In the case that tensile stress is applied to this material, strain partitioning occurs in coarse-grained regions

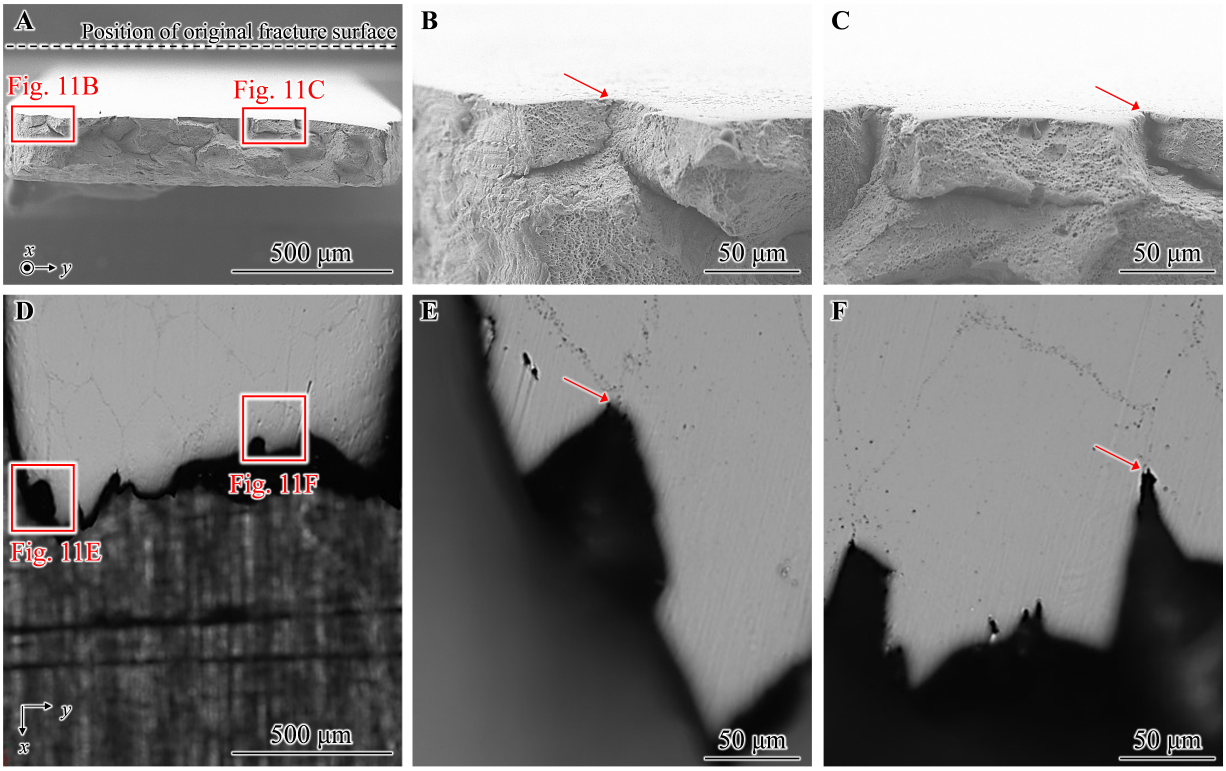


**Figure 11.** (A-C) SEM micrographs of fracture surface of polished Harmonic compact and (D-F) optical micrographs of specimen surface acquired at various magnifications in same field of view. Scanning electron microscopy.

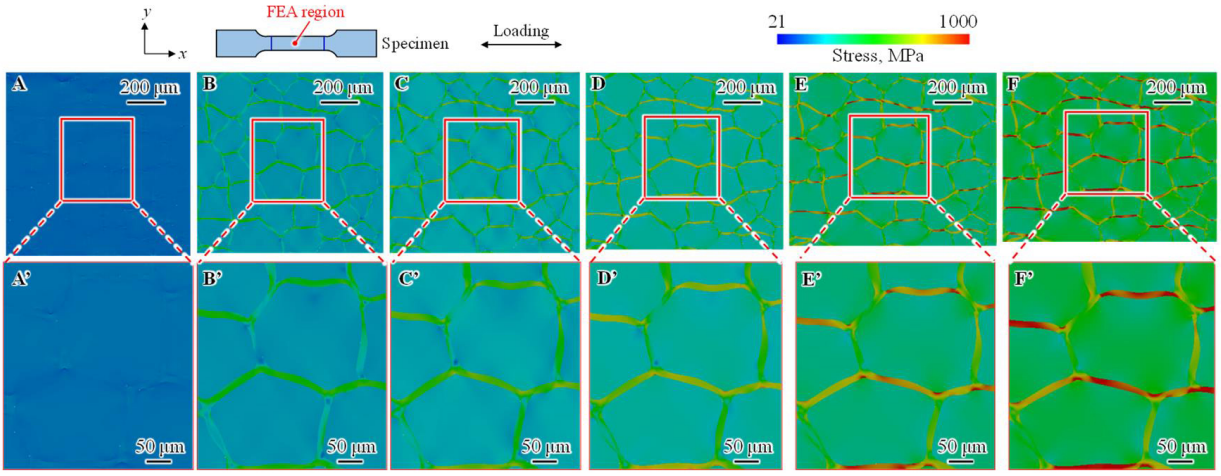


**Figure 12.** Equivalent stress maps obtained by FEA for Harmonic compact under various stress conditions corresponding to macroscopic strains of (A and A') 0.10%; (B and B') 0.59%; (C and C') 1.5%; (D and D') 3.8%; (E and E') 7.0% and (F and F') 10%. FEA: Finite element analysis.

exhibiting high ductility near the boundaries between fine- and coarse-grained structures [Figure 13ii]. As the tensile stress is increased, cracks are initiated within the fine-grained structures exhibiting high strength as a result of stress partitioning verified by FEA [Figure 13iii]. As a consequence of this mechanism, an HEA having an HS can exhibit both high strength and ductility. In future, it would be beneficial to assess the fatigue characteristics of such materials and to consider the use of additive manufacturing as a means of fabricating HEAs[17,25] having HSs.

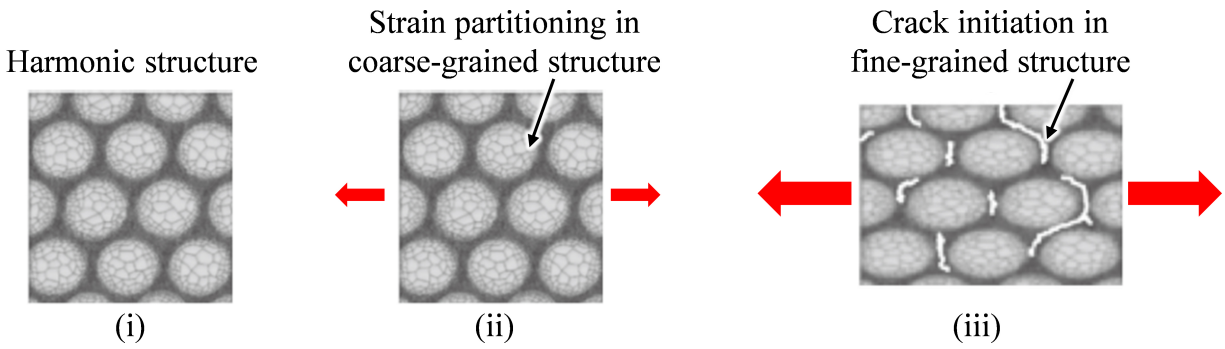


**Figure 13.** Diagram summarizing proposed fracture mechanism [(i) microstructure of HS; (ii) strain partitioning in coarse-grained structure and (iii) crack initiation in fine-grained structure] for HEA with HS based on micro-DIC analysis, fractography and FEA. HEA: High-entropy alloy; HS: harmonic structure; DIC: digital image correlation; FEA: finite element analysis.

## CONCLUSIONS

The present study examined the tensile deformation characteristics of a CrMnFeCoNi HEA having an HS based on *in situ* tensile tests combined with micro-DIC. The associated fracture mechanism resulting from monotonic tension was also assessed using fractography and FEA. The main conclusions can be summarized as follows.

(1) Imparting an HS to this alloy increases both the strength and ductility of the metal. The HS material exhibits both higher strength and elongation compared with that of an analogous alloy having a homogeneous coarse-grained structure.

(2) Micro-DIC analysis can be used to ascertain the strain distribution in an HEA having an HS under monotonic tension without dot patterning based on microstructural heterogeneity.

(3) The most important factor related to strain partitioning in an HS is the boundaries between coarse- and fine-grained structures. The second most important factor is the grain boundaries in the HS.

(4) Cracks tend to initiate within the fine-grained regions of such materials in response to monotonic tension due to stress partitioning.

## DECLARATIONS

### Authors' contributions

Made substantial contributions to conception and design of the study and performed data analysis and interpretation: Kikuchi, S.
Performed data acquisition and data analysis: Baba, S.; Katsumata, M.
Technical and material support: Kawabata, M. O.; Fujiwara, H; Ameyama, K.

### Availability of data and materials

The original contributions presented in this study are included in the article. Further inquiries can be directed to the corresponding author.

### AI and AI-assisted tools statement

Not applicable.

### Financial support and sponsorship

This work was supported by JSPS KAKENHI Grant (No. 22KJ1505, 23K22630 and 24H00846) and PRESTO, Japan Science and Technology Agency (No. JPMJPR2093).

### Conflicts of interest

All authors declared that there are no conflicts of interest.

## Ethical approval and consent to participate

Not applicable.

## Consent for publication

Not applicable.

## Copyright



## REFERENCES


1. George, E.; Curtin, W.; Tasan, C. High entropy alloys: a focused review of mechanical properties and deformation mechanisms. *Acta. Mater.* **2020**, *188*, 435-74. DOI
2. Li, W.; Xie, D.; Li, D.; Zhang, Y.; Gao, Y.; Liaw, P. K. Mechanical behavior of high-entropy alloys. *Prog. Mater. Sci.* **2021**, *118*, 100777. DOI
3. Cantor, B.; Chang, I.; Knight, P.; Vincent, A. Microstructural development in equiatomic multicomponent alloys. *Mat. Sci. Eng. A-Struct.* **2004**, *375-377*, 213-8. DOI
4. Otto, F.; Dlouhý, A.; Somsen, C.; Bei, H.; Eggeler, G.; George, E. The influences of temperature and microstructure on the tensile properties of a CoCrFeMnNi high-entropy alloy. *Acta. Mater.* **2013**, *61*, 5743-55. DOI
5. Gludovatz, B.; Hohenwarter, A.; Catoor, D.; Chang, E. H.; George, E. P.; Ritchie, R. O. A fracture-resistant high-entropy alloy for cryogenic applications. *Science* **2014**, *345*, 1153-8. DOI PubMed
6. Liu, W.; Wu, Y.; He, J.; Nieh, T.; Lu, Z. Grain growth and the Hall-Petch relationship in a high-entropy FeCrNiCoMn alloy. *Scr. Mater.* **2013**, *68*, 526-9. DOI
7. Sun, S.; Tian, Y.; Lin, H.; et al. Enhanced strength and ductility of bulk CoCrFeMnNi high entropy alloy having fully recrystallized ultrafine-grained structure. *Mater. Design.* **2017**, *133*, 122-7. DOI
8. Watanabe, H.; Murata, T.; Ikeo, N.; Mukai, T.; Han, K.; Tsuchiya, K. Effect of initial microstructure on grain refinement under hot compression in CrMnFeCoNi high-entropy alloy with Al addition. *Materialia* **2021**, *18*, 101172. DOI
9. Li, X.; Liu, R.; Hou, J.; Zhang, Z.; Zhang, Z. Trade-off model for strength-ductility relationship of metallic materials. *Acta. Mater.* **2025**, *289*, 120942. DOI
10. Ma, E. Instabilities and ductility of nanocrystalline and ultrafine-grained metals. *Scr. Mater.* **2003**, *49*, 663-8. DOI
11. Dong, X.; Gao, B.; Xiao, L.; et al. Heterostructured metallic structural materials: research methods, properties, and future perspectives. *Adv. Funct. Mater.* **2024**, *34*, 2410521. DOI
12. Fang, T. H.; Li, W. L.; Tao, N. R.; Lu, K. Revealing extraordinary intrinsic tensile plasticity in gradient nano-grained copper. *Science* **2011**, *331*, 1587-90. DOI PubMed
13. Wang, Y.; Chen, M.; Zhou, F.; Ma, E. High tensile ductility in a nanostructured metal. *Nature* **2002**, *419*, 912-5. DOI PubMed
14. Zhu, Y.; Wu, X. Heterostructured materials. *Prog. Mater. Sci.* **2023**, *131*, 101019. DOI
15. Park, K.; Nishiyama, M.; Nakada, N.; Tsuchiyama, T.; Takaki, S. Effect of the martensite distribution on the strain hardening and ductile fracture behaviors in dual-phase steel. *Mat. Sci. Eng. A-Struct.* **2014**, *604*, 135-41. DOI
16. Lee, K.; Song, Y.; Kim, S.; et al. Genetic design of new aluminum alloys to overcome strength-ductility trade-off dilemma. *J. Alloys. Compd.* **2023**, *947*, 169546. DOI
17. Yang, Y.; Hu, J.; Liu, X.; et al. Post treatment of an additively manufactured composite consisting of 304L stainless steel and CoCrFeMnNi high-entropy alloy. *Mat. Sci. Eng. A-Struct.* **2022**, *831*, 142104. DOI
18. Shokry, A.; Ståhle, P.; Orlov, D. On the optimisation of phase fractions in harmonic structure materials. *J. Mater. Sci.* **2024**, *59*, 6115-33. DOI
19. Ameyama, K.; Cazes, F.; Couque, H.; et al. Harmonic structure, a promising microstructure design. *Mater,. Res. Lett.* **2022**, *10*, 440-71. DOI
20. Orlov, D.; Kulagin, R.; Beygelzimer, Y. Strain partitioning and back-stress evaluation in harmonic-structure materials. *Mater. Lett.* **2020**, *275*, 128126. DOI
21. Sathiyamoorthi, P.; Kim, H. S. High-entropy alloys with heterogeneous microstructure: Processing and mechanical properties. *Prog. Mater. Sci.* **2022**, *123*, 100709. DOI
22. Shi, L.; Zhang, Z.; Chen, X. Fatigue crack growth behavior in CoCrFeMnNi high entropy alloy with harmonic structure topology. *Int. J. Fatigue.* **2023**, *172*, 107656. DOI

23. Tokizane, M.; Isonishi, K. Production of uniformly-sized spherical powder by plasma rotating electrode process and its applications to some intermetallics powders. *J. Jpn. Soc. Powder. Powder. Metallurgy.* **1992**, *39*, 1137-44. DOI
24. Zhu, Y.; Wu, X. Perspective on hetero-deformation induced (HDI) hardening and back stress. *Mater. Res. Lett.* **2019**, *7*, 393-8. DOI
25. Hayashi, M.; Kurita, N.; Watanabe, T.; et al. Effects of defects and shot peening on fatigue properties of additively manufactured CoCrFeNiTiMo-based high-entropy alloys. *J. Mater. Eng. Perform.* **2024**, *33*, 13916-23. DOI